



Microfluidic multi-target sorting by magnetic repulsion

Saud A. Khashan¹ · Sawsan Dagher² · Anas Alazzam^{3,4}

Received: 18 March 2018 / Accepted: 24 May 2018 / Published online: 6 June 2018
© Springer-Verlag GmbH Germany, part of Springer Nature 2018

Abstract

In magnetophoresis-based microfluidic systems, the free-flow sorting is achieved by incrementally navigating the magnetic target toward a designated outlet. This is typically enabled using high-gradient magnetic concentrators (HGMCs), axially aligned or slightly slanted with the streaming sample flow. Such axial and incremental magnetic manipulation critically constrains the throughput and the number of targets that can be sorted simultaneously. To overcome these constraints, we present an alternative repulsion-based sorting method. The repulsion force is due that induced, over a limited angular expanse, around a single ferromagnetic wire. The wire is positioned transversally against the focused sample flow. Differentially repelled by the repulsive force, each target deflects from its focused path to follow a ribbon-like trajectory that leads to a spatially addressable outlet. The mediated sorting takes place more rapidly and is confined to the region facing the transversal wire. More importantly, the introduced concept design allows for a throughput that is geometrically scalable with the length of the wire. The functionality of the systems is demonstrated experimentally and numerically to yield the simultaneous and complete multi-target sorting of two and more magnetic beads.

1 Introduction

Developing microfluidic bioassays to sort cells or other biological entities simultaneously and at high throughput will pave the ways for effective extraction, purification, enrichment, and depletion applications. For free-flow, multi-target sorting to be effective, the target entities must be steered concurrently and precisely to their corresponding processing or collection/detection sites, with high purity and recovery rates (Adams and Soh 2009; Kim and Soh 2009). The distinctive interaction with the magnetic forces and with the

ambient fluid offers a great opportunity to design systems aimed at the sorting of magnetic entities. These entities can be inherently magnetic or magnetically labeled with functionalized magnetic particles based on their surface expressions and binding capacities (McCloskey et al. 2003; Alazzam et al. 2017). In that contest, hard magnetic elements, while lacking the switching-on and -off controllability, have been successfully utilized to perform free-flow sorting (Pamme and Manz 2004; Vojtíšek et al. 2012). In addition, microfabricated coils have been used to generate the electrically switchable, but weaker, magnetic force needed for binary sorting (Kong et al. 2011; Ramadan et al. 2009).

The passive techniques utilizing high-gradient magnetic separation (HGMS) proved practicality in many free-flow magnetophoresis-based biomicrofluidics, especially those intended for immunomagnetic separation (IMS) applications. High-gradient magnetic concentrators (HGMCs) can be used to generate localized magnetic field, and, therefore, induce the magnetic force required to drive magnetically labeled biomolecules, with different magnetophoretic mobilities, toward spatially addressable outlets distinct from those carrying other magnetic or nonmagnetic molecules (Adams and Soh 2009; Kim and Soh 2009; Hoyos et al. 2000).

Despite all the success in separating or sorting magnetic entities, the existing HGMS-based free-flow micro-devices have a major drawback to overcome; their existing

Electronic supplementary material The online version of this article (<https://doi.org/10.1007/s10404-018-2083-z>) contains supplementary material, which is available to authorized users.

✉ Saud A. Khashan
skhashan@just.edu.jo

¹ Department of Mechanical Engineering, Jordan University of Science and Technology, P.O. Box 3030, Irbid 22110, Jordan

² Department of Mechanical Engineering, UAE University, Al Ain, UAE

³ Department of Mechanical Engineering, Khalifa University, Abu Dhabi, UAE

⁴ Electrical Engineering Department, École de Technologie Supérieure, Montreal, Canada

design cannot be geometrically scaled-up to handle higher throughputs. These systems utilize the axial magnetic arrangement; the HGMCs wires are invasively aligned with the sample flow direction (Han and Bruno Frazier 2004), or non-invasively patterned with an angle to that sample flow (Inglis et al. 2004; Lou et al. 2009; Adams et al. 2008). The induced magnetic force incrementally attracts the magnetic targets, flowing alongside the HGMC, from their initial flow path toward free-flow sorting outlet. With that, their magnetic operation is based on incrementally attracting paramagnetic or superparamagnetic targets toward magnetic attraction lines (i.e., magnetic field maxima) corresponding to wire-like ferromagnetic structures, or by repelling diamagnetic target out of these lines (Han and Bruno Frazier 2004). For binary sorting, two sets of microfabricated ferromagnetic strips, embedded beneath the streaming flow, were used (Adams et al. 2008); each target was steered toward a corresponding outlet using a differentially slanted set. This length-wise incremental attraction must take place cross-wise a co-flowing sheath flow. In addition to focusing, the sheath flow aids the combined magnetic and hydrodynamic steering of the target toward their corresponding outlets, and prevents targets from agglomerating on, or near, the HGMC. For the effective force is only within tens of microns from these elements, targets outside the force reach would be streaming without tangible magnetic manipulation. With that, these systems cannot be geometrically scaled-up, i.e., geometrically extended far away from the attractive lines, without compromising the desired level of magnetic selectivity. Being geometrically scalable, throughput can be increased by increasing the cross-sectional area without having to increase the velocity of the introduced sample.

Virtually all sorting applications, especially those involving immunomagnetic cell sorting, will benefit from an increase in the throughput. Developing multi-target sorting systems that allow for a geometrically scalable throughput can help cut both the processing time and the cost associated with many existing methods. As such is the need, our motive was to realize a system that can be geometrically scaled up for higher throughput whilst maintaining the ability to precisely sort micro-entities of distinct magnetic susceptibilities. Here, we demonstrate that such favorable concept designs are feasible by utilizing the HGMC as a transversal repulsive barrier. This transversal barrier sorts multi-targets, differentially and rapidly, by deflecting them laterally from their streaming direction toward their designated sorting outlets. Unlike with the incremental and axial attraction-based operations, the sorting system, introduced here, mediates sorting by the rapid and confined repulsion caused by a transversal HGMC.

2 Theory

2.1 Transversal magnetic arrangement

In the transversal magnetic arrangement, shown in Fig. 1, the flow direction, the applied external magnetic field, and the single ferromagnetic wire are all reciprocally perpendicular. When exposed to a uniform one-dimensional external magnetic field, $\mathbf{H}_0 = H_0 \mathbf{e}_y$, the magnetic scalar potential, φ , around a circular ferromagnetic wire with a radius a and centered at $(0, 0)$ can be described as (Han and Bruno Frazier 2004; Han et al. 2005).

$$\varphi = -H_0 y + k H_0 a^2 \frac{y}{(x^2 + y^2)}, \quad r = \sqrt{x^2 + y^2} > a. \quad (1)$$

With the magnetic permeability of the ambient fluid is approximately equal to that of the free space (μ_0), we have,

$$k = \frac{\mu_w - \mu_0}{\mu_w + \mu_0}, \quad (2)$$

where μ_w is the magnetic permeability of the ferromagnetic wire. Since $\mathbf{H} = -\nabla \varphi$ (non-rotational field), the induced magnetic field by the wire can be expressed as:

$$\mathbf{H} = \frac{H_0}{(x^2 + y^2)^2} \left[[2a^2 kxy] \mathbf{e}_x + [(x^2 + y^2)^2 - a^2 k(x^2 - y^2)] \mathbf{e}_y \right]. \quad (3)$$

Here a uniform one-dimensional external magnetic induction field ($B_0 \mathbf{e}_y = \mu_0 H_0 \mathbf{e}_y$) becomes non-homogenous and two-dimensional in the nearby of a long ferromagnetic wire. Figure 2a shows the induced magnetic intensity when the external field ($B_0 = 0.5 \text{ T}$) is applied transversal to the axis of a ferromagnetic wire. The induced magnetic polarity on that

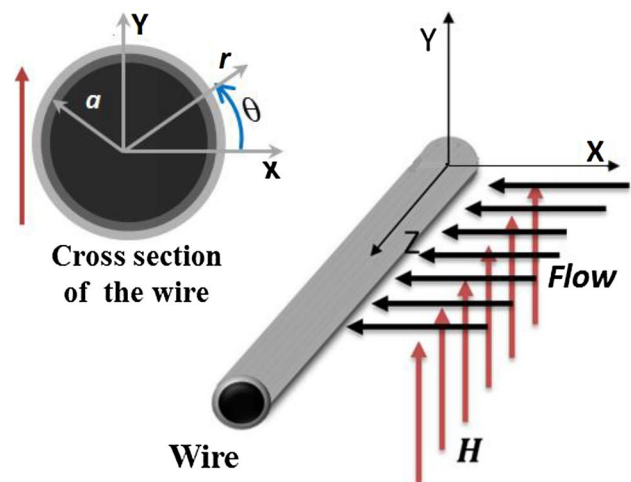


Fig. 1 Two- and three-dimensional view of the used ferromagnetic wire with respect to the external magnetic field and flow direction

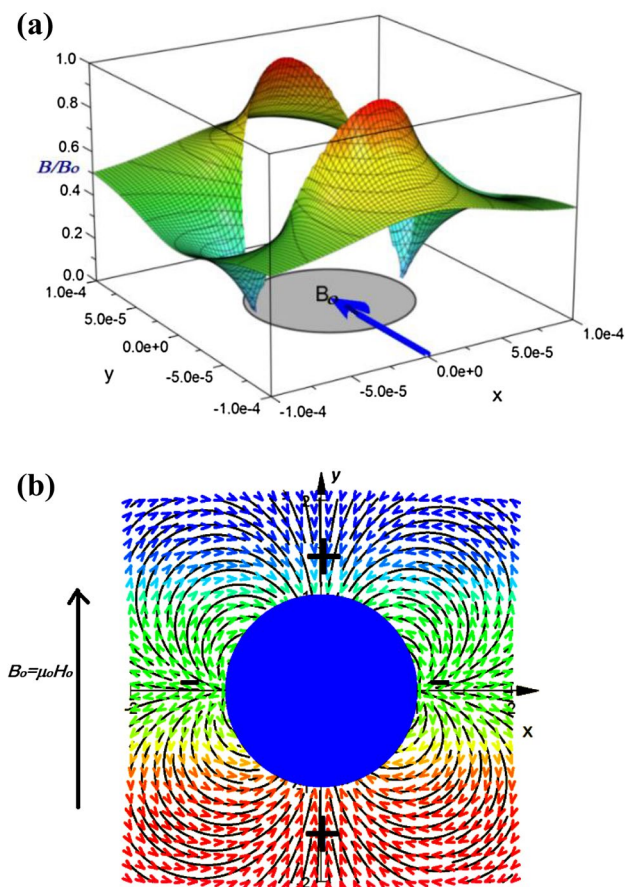


Fig. 2 **a** Surface plot and contours of the scaled magnetic flux intensity B/B_0 ($B_0=0.5$ T) acting on a Myone™ bead (1.0- μm) in the x - y plane outside the long ferromagnetic wire. The wire is subjected to a uniform external magnetic field ($B_0=0.5$ T) along the y -direction. Here, B/B_0 varies in the minimum 0.067 (blue) to the maximum 1.93 (red). **b** The acting magnetic force vectors superimposed with the streamlines that suspended Myone™ beads follow in the absence of fluid drag resistance. The +ve sign marks the attractive region and the -ve sign marks the repulsive region

wire creates low- and high-field regions resulting in opposite magnetic field gradients.

2.2 Particle dynamics

Assuming the magnetic particle as a point-like magnetic dipole, the acting magnetic force on the particle can be expressed as:

$$\mathbf{F}_m = \frac{1}{2} \mu_0 \chi V_p \nabla H^2. \tag{4}$$

For the induced magnetic field described by Eq. (3), the magnetic force components are (Han et al. 2005; Han and Bruno Frazier 2004):

$$F_{mx} = -2\mu_0 \chi V_p H_0^2 a^2 k \frac{(ka^2 - x^2 + 3y^2)x}{(x^2 + y^2)^3}, \tag{5}$$

$$F_{my} = -2\mu_0 \chi V_p H_0^2 a^2 k \frac{(ka^2 - 3x^2 + y^2)y}{(x^2 + y^2)^3}. \tag{6}$$

Based on the wire’s saturation magnetization M_{ws} , k can be expressed for both magnetically non-saturated and magnetically saturated conditions as (Fletcher 1991; Han et al. 2005):

$$k = \begin{bmatrix} 1.0 & \text{if } H_0 \leq \frac{M_{ws}}{2}; \text{ (non-sat)} \\ \frac{M_{ws}}{2H_0} & \text{if } H_0 > \frac{M_{ws}}{2}; \text{ (sat)} \end{bmatrix}. \tag{7}$$

Figure 2b shows the acting magnetic force vectors (arrows) and the streamlines (solid lines) that the freely suspended Myone™ bead (1.0- μm) would follow in a frictionless motion (far from walls). It is clear that the streamlines closely follow the generated magnetic force vectors. Obviously, for a flowing sample, the particle–fluid- and particle–wall interactions will disturb the symmetrical streamlines significantly.

The particles, driven by magnetic force, move at velocities different from the ambient fluid. The relative velocity comes as a result of the magnetophoretic mobility attained when the magnetic force is strong enough to overcome the drag (or other body or surface forces) imposed by the ambient fluid. In principle, the forces acting on a magnetic particle can be due to other influences. For microparticles in a state of dilute suspension within an ambient liquid with comparable density, the forces due Brownian motion, lift, and particle–particle interactions are very small and can be neglected (Khashan and Furlani 2012; Khashan et al. 2014). The particle’s motion can be described as,

$$m_p \frac{d\mathbf{u}_p}{dt} = 6\pi\eta a (\mathbf{u} - \mathbf{u}_p) + \mathbf{F}_m, \tag{8}$$

where m_p and \mathbf{u}_p are the mass and the velocity of the particle; \mathbf{u} , η are the velocity and viscosity of the ambient fluid; a and V_p are the radius, and volume of the particle; and \mathbf{g} is gravity field. The first term on the right-hand side of Eq. (8) accounts for the drag on the particle and the second for the magnetic forces, respectively.

The temporal trajectory positions, $\mathbf{x}_p(t)$, can be described by the kinematic equation,

$$\frac{d\mathbf{x}_p}{dt} = \mathbf{u}_p. \tag{9}$$

2.3 Repulsion action: an exploratory experiment

The repulsive action, attained by the axial arrangement, and the effect of hydrodynamic focusing were examined using a relatively simple experimental set-up. Both unfocused and focused sample streams, carrying a single type of magnetic beads, were injected toward a Permalloy wire (ESPI Metals, USA) with 0.254 mm in diameter. The wire is set invasive and transversal to the injected sample. The applied external magnetic field is due to a disc Neodymium Iron Boron (NdFeB) Magnet; grade N52, (D12 × 3 mm, 1.48 T, Neomagnete, Germany) with its magnetization axis parallel to the 3 mm direction. The trajectories of magnetic beads for both unfocused and focused injections are shown in Fig. 3. The unfocused injection exemplifies the attraction force induced by a single wire (collector) of an array of many wires, commonly used for magnetic filtration (Ying et al. 2000; Eisenträger et al. 2014). In these studies, the repulsion force was studied, only, in the context of their capture performance as attained at the attractive regions. Magnetic beads, focused toward the center of the repulsive side of the wire, were observed to be deterred from approaching this flow-facing side (around $\theta = 0^\circ$ in Fig. 1) to eventually get attracted by the upper and lower sides (i.e., near $+90^\circ$ and -90° , respectively) where the vertical attraction forces are dominant. In a previous study (Khashan et al. 2017a, b), similar experiments were conducted for particles with larger magnetic content and revealed that the repulsion starts on a further distance from the wire.

2.4 Sorting mechanism

The sorting functionality relies, here, simply on the fact that magnetic targets, when focused precisely toward the

repulsive side of a flow-traversing HGMC, will experience differential repulsive deflections according to their distinct magnetic responses with this repulsive barrier. This barrier is formed because of the magnetic polarity attained around the HGMC; repulsive field minima are forming over a limited angular expanse on the sides facing the flow direction and attractive field maxima are forming on the side normal to the external magnetic field. It is worth mentioning that an opposite attractive/repulsive forces behavior would form if the magnetic susceptibility of the particle were negative (i.e., diamagnetic). In such a case, the system can be utilized in diamagnetic capture modes (Han et al. 2005). However, the repulsive force experienced by a magnetic particle, in this study, has the same order of magnitude as the attractive force while the repulsive force experienced by diamagnetic particles is several orders of magnitude weaker.

The main advantage of this arrangement over axial ones is allowing more rapid and regionally confined sorting with a throughput that is scalable with the length of the wire inside the microdevice. With that, the volumetric pumping can be scaled-up by extending the size of the sorting system while maintaining the full utility of the short-ranged repulsive force, without having to increase the velocity of the introduced sample. For a circular ferromagnetic wire, in the presence of a uniform magnetic field, the repulsive magnetic force exists over a limited angular expanse of its circumference. Therefore, to ensure the rapid differential deflections, the sample flow must be hydrodynamically focused toward the center of that repulsive side; the wire must be larger than the focused stream.

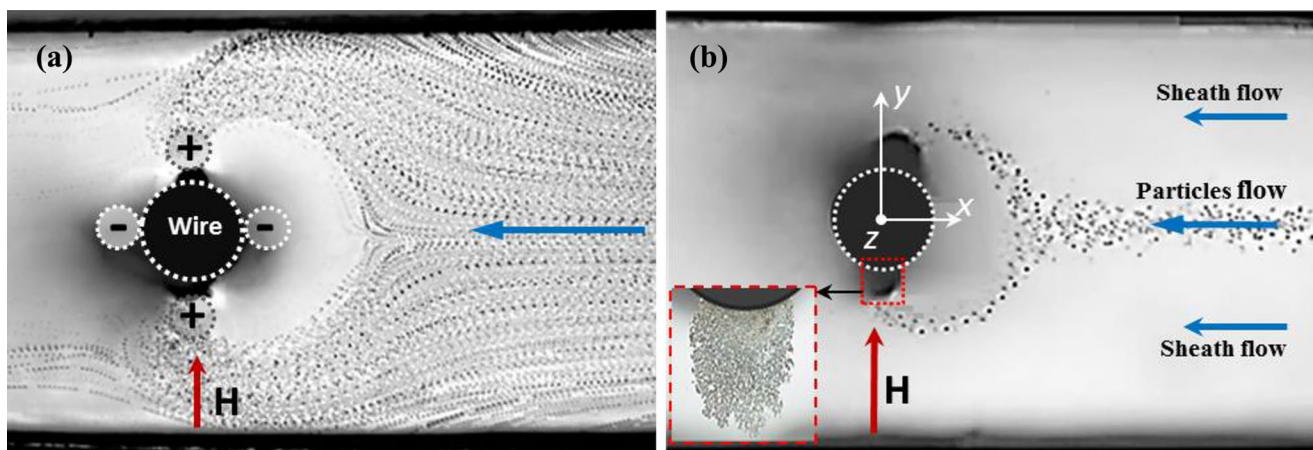


Fig. 3 Brightfield microscopic superimposed images of magnetic particles with diameters of 4.3 μm under a transversal magnetic arrangement for **a** unfocused sample flow at 4 $\mu\text{l/s}$. The positive sign

indicates the high magnetic field gradient side and the negative sign indicates the low magnetic field gradient side, **b** focused sample flow at 1.0 $\mu\text{l/s}$ and a sheath flow of 3.0 $\mu\text{l/s}$

3 Methods and materials

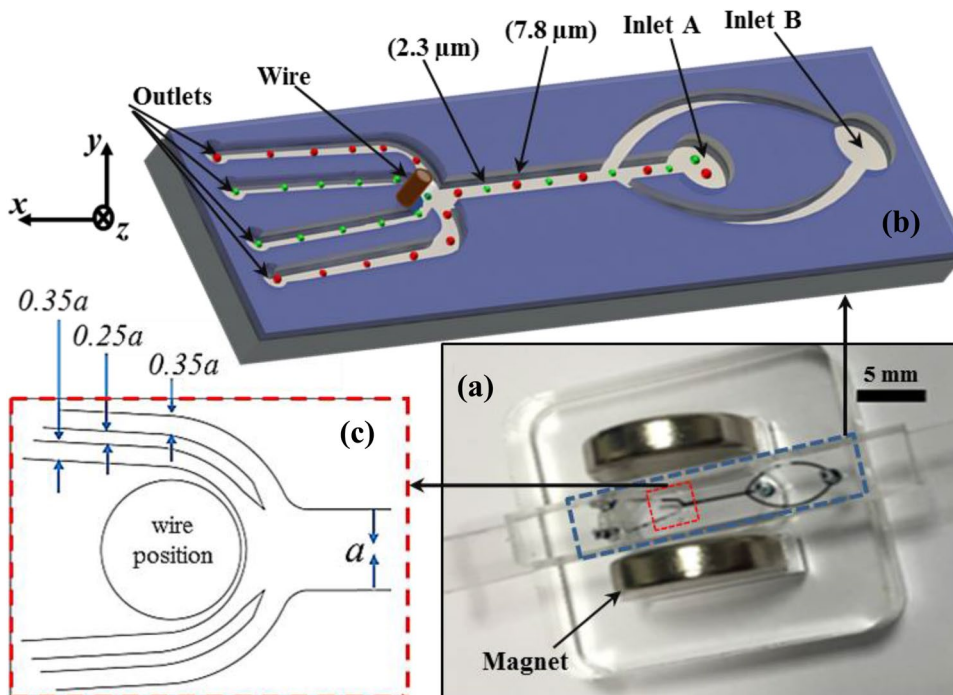
3.1 System design and experimental setup

The objective, here, is to deflect targets into defined free-flow trajectories and not to capture them. Thus, the geometry and the positioning of the sorting outlets, as well as, the thickness of the focused sample flow (with respect to the non-invasive wire) must be set to yield maximize repulsive forces while, at the same time, avoid the attractive forces at the top and bottom sides of the wire. The previous experiment indicates that the targets must be focused onto the repulsive region acting over a small angular span of the wire. With that, the outlets must start at locations confirming with the differential paths taken by the deflected targets. Nonetheless, one must not rely solely on the differing susceptibilities or magnetic saturation to ensure the distinct magnetic effect; these differences can be offset by hydrodynamics effects leading to similar magnetophoretic mobilities. Therefore, the distinctive steering parameters for of a magnetic particle must take into consideration the combined effects of its volume and magnetic properties.

Based on the aforementioned exploratory experiment (Fig. 3), we envisaged a multi-target sorting system that utilizes the highly localized magnetic repulsion induced by the transversal arrangement and in which sorting outlets were incorporated to confirm with the differential magnetophoretic mobility of each target. To take benefit of symmetry (with respect to the wire), the numerical simulation

(described later) indicates that the outlets must be curved up to bypass the wire’s attraction field. With that, the fabricated system (shown in Fig. 4) includes a main channel with opposed inlet and outlet ends, extending along the longitudinal (x) axis. The main channel starts with a focusing junction and ends with a sorting end. The clear buffer (pure-deionized water) and the sample (spherical magnetic particles functionalized with a carboxyl group [Spherotech Inc., USA], with mean diameters of 7.85 and 2.35 μm , suspended in deionized water) were driven by a syringe pump (Nemesys, NEM-B101-02E, Germany) from inlet A and inlet B independently at controlled flow rates. The buffer port at B branches symmetrically to enter, via two side inlet channels, the four-way focusing junction. The sample injected at A , passes through this focusing junction along the longitudinal direction. Focusing, as envisaged by Fig. 3b is essential to laminate the sample flow into a thin-layer streaming precisely toward the repulsive side of the wire near the sorting end. First and second outlet channels are disposed near the sorting end of the main channel. The first and second outlet channels have concentrically elliptical configurations with the first outlet channel has a larger curvature than the second outlet. Each of the first and second outlet channels is in fluid communication with each other. In proximity to the sorting end, the ferromagnetic wire is inserted transverse, but not invasive, to the sample flow. An external magnetic field was applied by two disc NdFeB magnets, grade N52 (D12 \times 3 mm, 1.48 T, Neomagnete, Germany), magnetized axially through its 3-mm thickness. The wire is transversely and symmetrically positioned mid-distance between the

Fig. 4 **a** Actual size photograph of the sorting device, scale bar=5.0 mm. Marking ink was used to help visualize the microfluidic channel. **b** Schematic diagram of the device (not to scale). **c** The dimensions of the main channel and the outlet channels



two magnets: the North Pole facing the South Pole (12 mm side). As such, almost a uniform external magnetic field was applied perpendicular to both of the flow (x direction) and to the long axis of the wire (z axis).

The device was fabricated using photolithography technique; an inverse structure (mold) defining the microchannel features is fabricated from SU8 photoresist on a silicon substrate. We replicated this mold by a soft-lithography technique, using PDMS, to produce the microchannels structures, with 300- μm thickness. A pre-fabricated Permalloy wire (ESPI Metals, USA), with 254 μm in diameter, was inserted through a punched hole crossing the whole depth (z -direction) of the device. Holes for wire insertion, inlets, and outlets for the fluid flow connections were punched using a sharpened medical puncher. Tubing (Tygon micro-bore 0.020" \times 0.060" OD, Cole Parmer, USA) and reservoirs were then connected to the access holes, allowing solutions to be introduced and collected. The two magnets were kept at the two sides of the main channel with 8 mm distance from each other (Fig. 4). It is aimed to have a minimum of 0.5 T acting on the wire. The flow in the chip was monitored near the sorting end by an optical microscope (OLYMPUS, IX83 research inverted microscope 2DECK, Japan) equipped with a camera (Olympus, DP 73). The particle-sorting process was tracked digitally using stacked images (15 fps) at 10 \times magnification (Olympus cellSensTM). More details about the device and the fabrication method, as well as sample preparation, are included in the supplementary materials.

The induced repulsive force deflects magnetic targets, according to their distinctive magnetic response, into distinct paths that lead them to spatially addressable outlets. The distinct magnetic and hydrodynamic responses by each particle type dictate the starting position and the degree and rapidity of its deflection. The deflected path of each target must be confined to follow a designated route. The target particles may then be collected and/or immobilized for detection or surface processing. Furthermore, the sorting outlets must be designed carefully so as targets can escape the attractive force induced in the other parts of the HGMC (the two sides facing the external magnetic field).

3.2 Numerical method

Reliable numerical simulations help focus the fabrication and experimental efforts on, more likely, functional designs. With that in mind, the experimental set-up, as described in the previous section, was led by the simulation results for a variety of concept designs. Here, we describe the simulation setup of a two-dimensional concept design that closely, though not strictly, resembles that fabricated in the experimental study. We assumed the (transversal) depth of the microchannel, so the magnetic wire, to be considerably larger than its main plane dimensions. In addition to

simplicity, such 2D analysis becomes more relevant when the geometrical scalability (with the transversal depth) is pursued.

Focusing on the capture-based functionality, we reported in earlier works, a coupled Lagrangian–Eulerian CFD-based numerical model for simulating the transport of magnetic microparticles in magnetophoresis-based microfluidics. We used the model to assess the capture efficiency attained using magnetic dipole (Khashan and Furlani 2012); wall-embedded (Khashan and Furlani 2013) (Khashan and Furlani 2014; Khashan et al. 2017a, b) and flow-invasive (Khashan et al. 2015) rectangular ferromagnetic wires. We briefly describe the approach here, details of the model can be found in the references (Khashan and Furlani 2013, 2014). The Lagrangian analysis is used to track the motion of the (discrete) representative particles, parcels; Eqs. (8) and (9) were integrated numerically using the fourth-order Runge–Kutta method. The induced magnetic force, pertaining in this work to a circular magnetic wire, is as stated by Eqs. (3) and (4). The Eulerian-based CFD analysis, on the other hand, is used to solve the (continuous) mixture flow using the Navier Stokes equations. Two-way coupling between the particles and the ambient fluid is achieved by introducing a sink term in the fluid's momentum equations. This term (weighed by the particle concentration in the Eulerian computational cell) accounts for the momentum exchange between the discrete (particles) and the continuous (fluid) phases. The convergence is reached by alternately solving the discrete and continuous phase equations until subsequent calculations agree to within a prescribed tolerance. It must be noted that this approach differs from the Eulerian–Eulerian approach in which the bead transport is modeled by a mass diffusion equation (Khashan et al. 2011) or by an algebraic slip equation (Khashan et al. 2017a, b).

The computational domain (with respect to the magnetic arrangement) is shown in Fig. 5. The sample flow, comprising three types of magnetic beads and one type of non-magnetic beads carried by a buffer, enters through the middle inlet. The buffer enters the main channel laterally through two side channels, positioned symmetrically about the sample port. Close to the downstream-sorting end, the main channel branches laterally into three, cylindrically concentric, paired outlets. Since the properties of the magnetic beads and the pre-fabricated ferromagnetic wire, used in the experiment, were lacking, we selected MyoneTM (1- μm), M-280TM (2.8- μm) and M-450TM (4.5- μm) beads (Dynal Biotech) for the simulation. These beads have documented properties (Fønnum et al. 2005), (Adams et al. 2008), and are listed in the caption of Fig. 6. The (non-invasive) ferromagnetic wire is assumed as Permalloy (78% Ni, 22% Fe) with the saturation magnetization $M_{\text{es}} = 8.6 \times 10^5$ A/m. A uniform external field $H_0 = 3.9 \times 10^5$ A/m (0.5 T) is set perpendicular to both the flow (x direction) and to the long axis of the wire (z axis). This external field was found sufficient to saturate both the elements and the particles

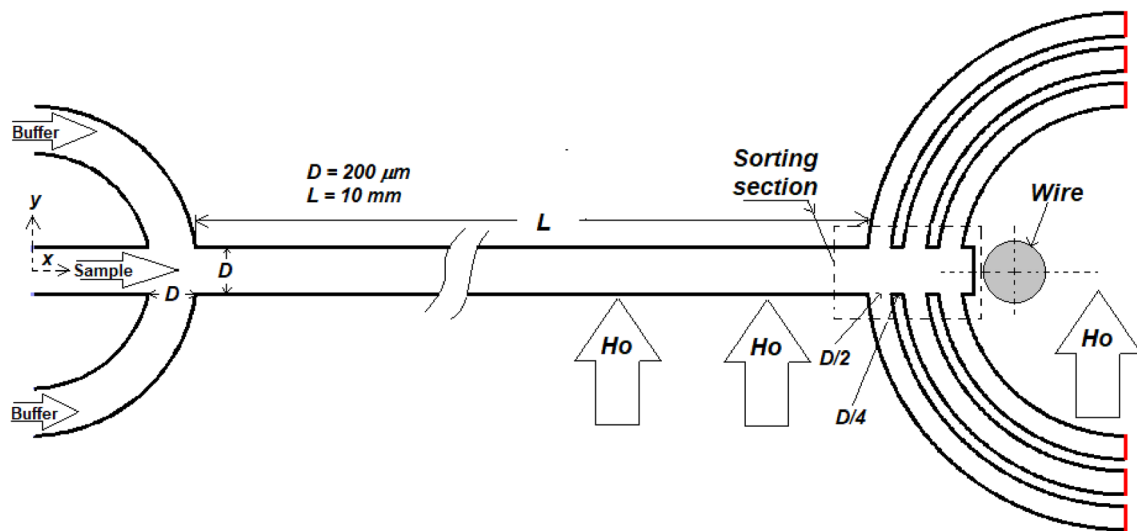


Fig. 5 The computational domain of the simulated concept design and the magnetic arrangement. The external magnet is perpendicular to the axial flow and to the transversal Permalloy wire

(Khashan and Furlani 2013, 2014). Similar to the experiment, the focusing buffer, as well as, the ambient buffer are taken to be water ($\eta = 0.001 \text{ kg/m s}$, $\rho_f = 1000 \text{ kg/m}^3$).

4 Results and discussion

4.1 Numerical simulation

Figure 6 shows the calculated trajectories (zoomed at the sorting end) for the three magnetic- and one non-magnetic-type beads. Figure 6a shows the results obtained with a 254- μm (dia) Permalloy wire. A complete sorting of the middle-sized M-280 and the smallest Myone beads was achieved, with each directly exiting through a corresponding outlet. Though separated from the remaining beads, only a part of the M-450 beads experienced enough deflection to directly enter through its intended outlet (from the end); the remaining part had to lose considerable momentum to the wall and reside much longer therein before entering the outlet. Practically, this indicates for their possible agglomeration. This sorting is obtained after tuning the inlet sample and inlet buffer velocities to 2.5 and 4 mm/s, respectively. For the two-dimensional 200- μm channel, these inlet velocities correspond to the flow rates of 0.5 $\mu\text{l/s}$ for the sample and 1.6 $\mu\text{l/s}$ for the focusing buffer. Focusing the sample flow into a close-fitting stream became evident, almost immediately, once passing the four-way focusing junction. The beads kept confined within the focused stream for the downstream sorting (Fig. 6). Such focused streaming is required to direct target particles to the location where the repulsive magnetic forces are significant. For the same fluidic chip,

design variables pertaining to the inlet conditions and to the magnetic arrangement (including the position and the size of the wire) can be used to control the sorting. Inlet velocities control the thickness of the focused stream; thickness decreases with increasing the buffer-to-sample flow rate ratio. Using a larger (254- μm) wire and with tuning the inlet velocities, Fig. 6b shows a complete sorting of the three magnetic beads. Here, all magnetic bead types entered their corresponding outlets directly without losing momentum to the channel walls.

Obviously, the geometrical scalability becomes evident as long as the induced magnetic field remains two-dimensional [i.e., with little transversal ($-z$) variations]. Having a pre-fabricated ferromagnetic wire (external to the fluidic chip) removes the fabrication problems, usually, persisting when integrating long and relatively large HGMCs within a micro-device. Moreover, having an external magnetic field directed uniformly perpendicular to this long wire is not difficult to accommodate.

4.2 Experimental

The particles are introduced into the middle inlet and hydrodynamically focused by sheath flows in the main focusing channel (Fig. 7). In the absence of an external magnetic field, the microparticles reached the end of the main channel and then exited through the second outlets (Fig. 7a). With the magnetic field (Fig. 7b), sorting of the larger (7.85 μm) from the smaller (2.37 μm) beads occurred due to their differential repulsion. Having higher magnetic content, the larger particles experienced a stronger repulsive force and, therefore, deflected from

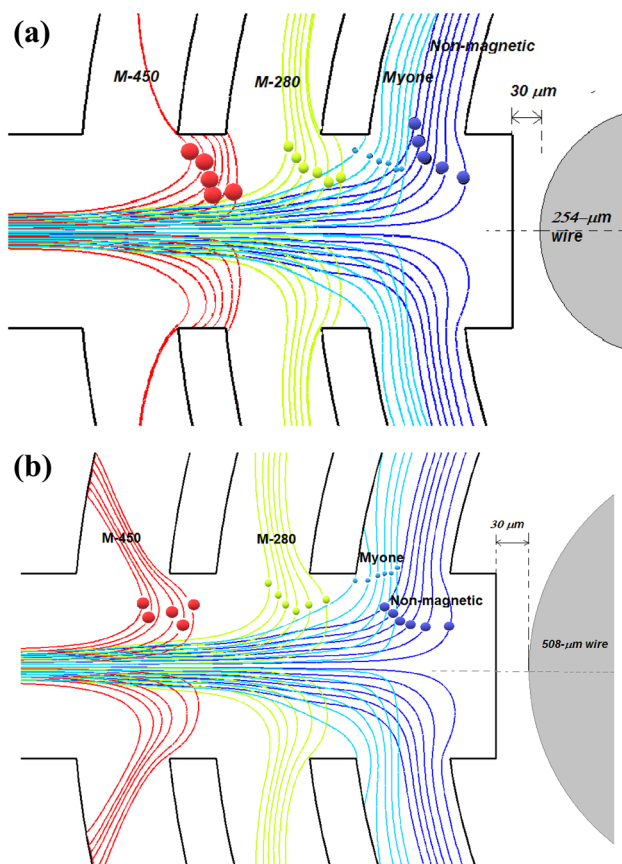


Fig. 6 Calculated bead trajectories near the sorting end. The buffer is water and the sample (carried by water) includes the beads: Myone ($d_p=1.05 \mu\text{m}$, $\rho=1791 \text{ kg/m}^3$, $\chi=1.43$); M-280 ($d_p=2.8 \mu\text{m}$, $\rho=1538 \text{ kg/m}^3$, $\chi=0.923$); M-450 ($d_p=4.5 \mu\text{m}$, $\rho=1578 \text{ kg/m}^3$, $\chi=1.58$); and non-magnetic beads ($d_p=1.0 \mu\text{m}$, $\rho=1800 \text{ kg/m}^3$, $\chi=0.0$). The trajectories are for: **a** $v_{\text{sample}}=2.0 \text{ mm/s}$, $v_{\text{buffer}}=3 \text{ mm/s}$, and $d_{\text{wire}}=254 \mu\text{m}$ distant $30 \mu\text{m}$ from the channel end; and **b** $v_{\text{sample}}=2.5 \text{ mm/s}$, $v_{\text{buffer}}=4 \text{ mm/s}$, and $d_{\text{wire}}=508 \mu\text{m}$ distant $30 \mu\text{m}$ from the channel end

their initial laminar flow paths towards the first side outlets. On the other hand, the repulsive force experienced by the smaller particles is lesser; they deflect at a closer distance from the wire to flow through the second outlets. For simplicity, we set the flows through the first and second outlets to end with a common vent. Therefore, sorting efficiency was monitored, here, only by the direct visualization attained from video streaming and from the recorded trajectories using stacked images; particles' counting is not attempted. The experiment was repeated several times and the sorting efficiency was found to be close to 100% for each run.

Figure 7b demonstrates the binary sorting performed at the sample flow rate of $0.10 \mu\text{l/s}$ (inlet A) and the buffer flow rate of $1.0 \mu\text{l/s}$ (inlet B). The separation distance between the wire and the end of the main channel is set to $40 \mu\text{m}$. Careful visualization of the particle trajectories indicates

that the repulsion force is strong enough to deflect all the larger beads to flow exclusively through the first outlet, i.e., the one with further distance from the wire. When the distance between the wire and the end of the main channel is increased from 40 to $80 \mu\text{m}$ (while keeping the same buffer flow rate), complete sorting was possible when the sample flow rate is decreased from 0.1 to $0.05 \mu\text{l/s}$ (Fig. 7c).

The effect of the flow rates on sorting efficiency was further investigated. For the sample flow of $0.05 \mu\text{l/s}$ but with the sheath flow is increased to $2 \mu\text{l/s}$ (i.e., twice of that corresponding to Fig. 7), some large particles (as shown in Fig. 8a) were dragged further inward against the repulsion force to find a way through the second outlet channels (i.e., closer to the wire). If the sheath flow is decreased to $0.5 \mu\text{l/s}$ (i.e., half of that corresponding to Fig. 7), part of the larger particles became stagnate or, at least, spent more residence time in the center of the main channel at a distance ranging between 120 and $150 \mu\text{m}$ from the wire (Fig. 8b). For the sheath flow of $1 \mu\text{l/s}$ and the low sample injection of $0.02 \mu\text{l/s}$, complete stagnation of the bigger particles occurred and the part of them flowing through the outlet reduced to none (see Fig. 8c). At least for the parameters corresponding to Fig. 7, effective continuous sorting can be achieved when the sample flow is set between 0.05 and $0.1 \mu\text{l/s}$ and the sheath flow is set between 0.7 and $1.0 \mu\text{l/s}$. Video and stacked images using another combination of particles (1.3 and $5.65 \mu\text{m}$ particles) are available in the supplementary materials.

To confirm the new concept design, another sorting device was developed. This design is like the previous design but with little modifications to the sorting end. Instead of being circular, the end of the main channel was concaved further towards the inside (see Fig. 9). The induced magnetic field was due to a larger wire ($d=0.508 \text{ mm}$) with the same permalloy material and the particle suspension was prepared similarly using different Spherotech beads; 1.30 - and 5.65 - μm in diameter. The sample containing the particles was introduced at $0.1 \mu\text{l/s}$ and was hydrodynamically focused by a $0.7 \mu\text{l/s}$ buffer flow. In the absence of a magnetic field, all particles reached the end of the main channel and then departed through the second outlets as shown in Fig. 9a. After applying the external magnetic field (Fig. 9b), the repulsive force, differentially, deflected the streaming particle types laterally, each to a corresponding outlet channel.

5 Conclusion

The sorting of multi magnetic targets, based on their differential repulsions from a single transversal HGMC, is demonstrated experimentally and numerically. By utilizing the transverse magnetic arrangement, the throughput can be geometrically scaled up, simply by extending the

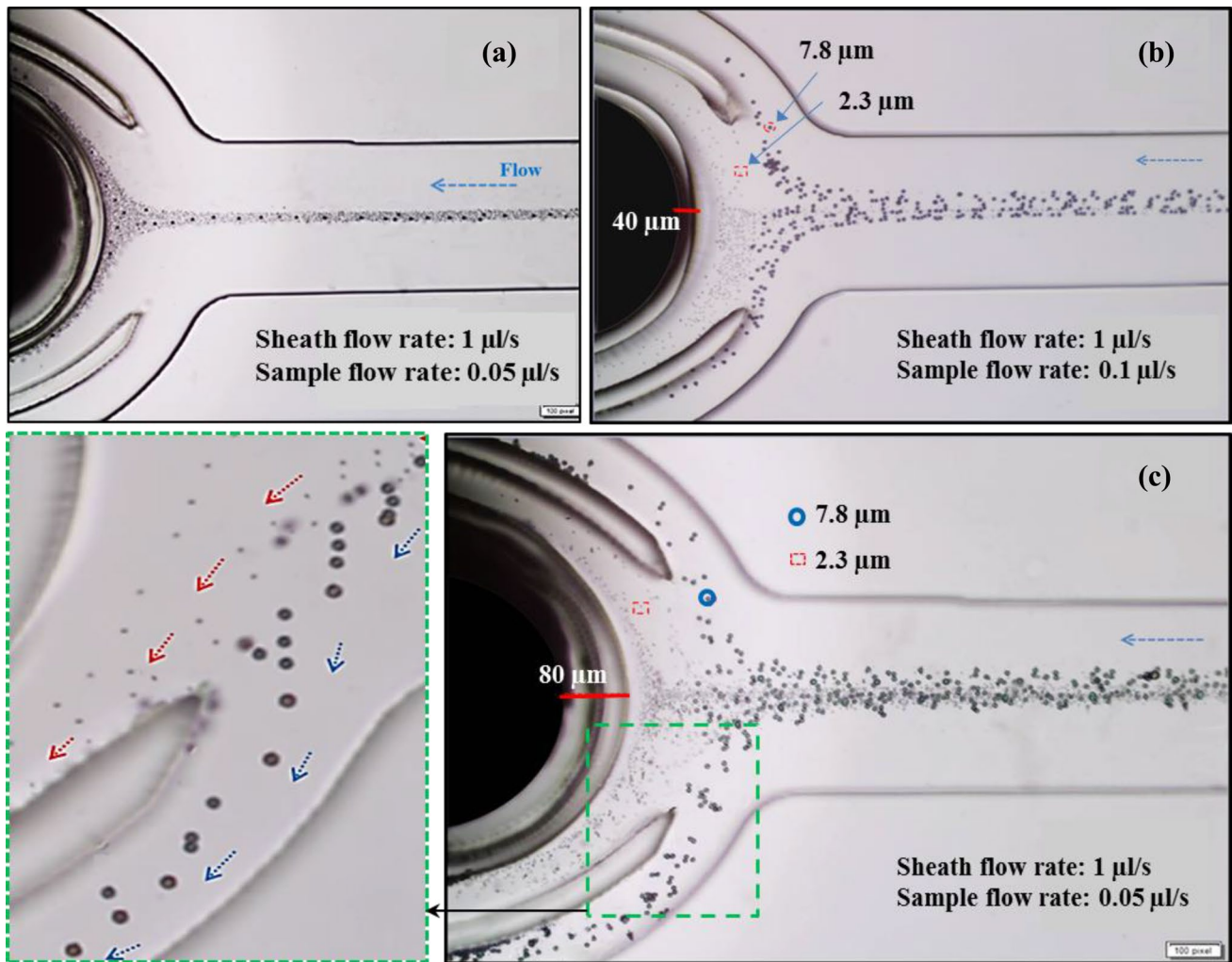


Fig. 7 Bright-field microscopic superimposed images of the magnetic particles at the sorting end of the microfluidic channel: **a** Absence of external magnetic field; **b, c** Presence of external magnetic field. Sorting demonstrated at a flow rate of 1.0 µl/s for the buffer, and 0.05 µl/s

or 0.1 for the sample, based on the separation distance between the wire and the end of the main channel. Video imaging is available with supplementary materials

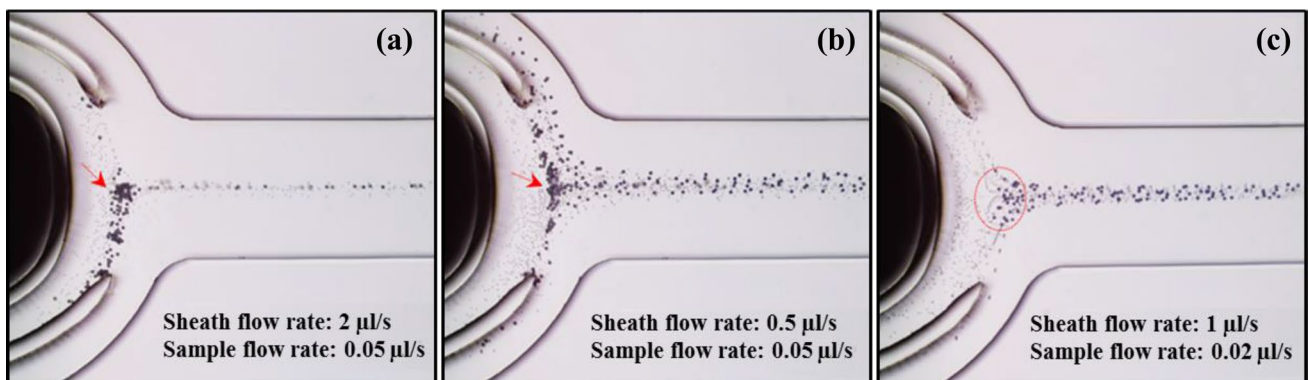


Fig. 8 Optical microscope superimposed images of the magnetic particle suspension in the microfluidic channel in the presence of magnetic field, at different flow rates (**a–c**). The arrows in (**a**) and (**b**) indicate the trapped 7.85 µm particles

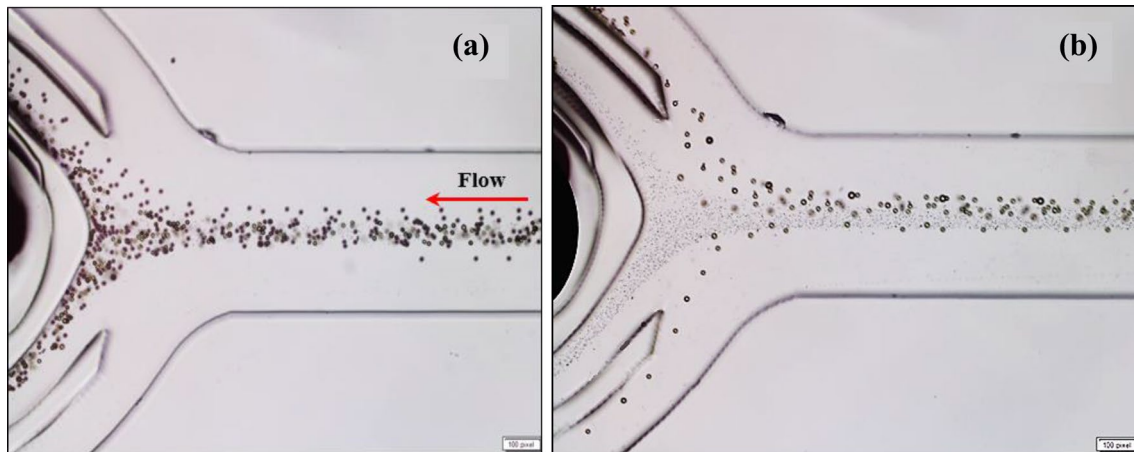


Fig. 9 Bright field microscopic superimposed images of magnetic particles with diameters of 1.30 and 5.65 μm in a 200 μm microfluidic channel in the **a** absence of magnetic field. **b** Presence of magnetic field, sorting demonstrated here was performed at a flow rate of;

0.7 $\mu\text{l/s}$ for the buffer, and 0.1 $\mu\text{l/s}$ for particles' suspension using a Permalloy wire with 0.508 mm diameter. The images are constructed by overlaying sequential frames (15 frames per second) of the corresponding time-lapse movies

microchannel depth along which the transversal non-invasive wire is aligned. With that, the channel can be configured to handle a layer of a hydrodynamically focused sample flow, with a macro-scaled width, whilst having the full utility of the short-ranged forces. Instead of the incremental magnetic operation that takes place with the wire when aligned alongside the flow, the developed system is set to sort the targets into ribbon-like sheets toward spatially addressable outlets. For the successful sorting, the introduced sample must be focused into a layer equal to or smaller than the angular span of the wire on which the repulsive force is forming. As alternatives for the hydrodynamics focusing used here, sheathless sample focusing can be achieved: inertially using a relatively long serpentine channel (Zhang et al. 2014); or by devising the sample with a viscoelastic behavior using a non-Newtonian aqueous buffer (Zhang et al. 2016). Although demonstrated experimentally here to sort two targets, the concept design, as demonstrated by the numerical simulation, can be configured to handle as many targets as the available designated outlets. With a closer wire and stronger induced repulsion field, the outlet nearest to the wire can be designated to vent, exclusively, all nonmagnetic particles. For the ferromagnetic wire is a pre-fabricated and with a large diameter (0.254 and 0.508 mm were used), the concept design introduced here, and a variety of its embodiments, allow for different types of wires to be mounted independently from the fluidic chip and to be controlled externally, like with a micropositioning stage. This will pave the way for building multiplexed HGMC-based micro-sorters that can be automated and reprogramed to serve a variety of integrated magnetic lab-on-chip biosensing systems.

Acknowledgements The authors are grateful for the help provided by Dr. Bobby Mathew in the lithographic mold fabrication at Khalifa University labs. The soft lithography and experiments were conducted using UAEU facilities.

References

- Adams JD, Soh HT (2009) Perspectives on utilizing unique features of microfluidics technology for particle and cell sorting. *J Lab Autom* 14(6):331–340. <https://doi.org/10.1016/j.jala.2009.06.003>
- Adams JD, Kim U, Soh HT (2008) Multitarget magnetic activated cell sorter. *Proc Natl Acad Sci* 105(47):18165–18170. <https://doi.org/10.1073/pnas.0809795105>
- Alazzam A, Mathew B, Khashan S (2017) Microfluidic platforms for bio-applications. In Zhang D, Wei B (eds) *Advanced mechatronics and MEMS devices II*. Springer International Publishing, Switzerland, pp 253–282. https://doi.org/10.1007/978-3-319-32180-6_12. <http://link.springer.com/>
- Eisenträger A, Vella D, Griffiths IM (2014) Particle capture efficiency in a multi-wire model for high gradient magnetic separation. *Appl Phys Lett* 105(3):033508. <https://doi.org/10.1063/1.4890965>
- Fletcher D (1991) Fine particle high gradient magnetic entrapment. *IEEE Trans Magn* 27(4):3655–3677. <http://www.scopus.com/inward/record.url?eid=2-s2.0-0026192484&partnerID=tZOtx3y1%5Cnhttp://ieeexplore.ieee.org/lpdocs/epic03/wrapper.htm?arnumber=102936>
- Fonnum G et al (2005) Characterisation of dynabeads[®] by magnetization measurements and Mössbauer spectroscopy. *J Magn Magn Mater* 293(1):41–47. <https://doi.org/10.1016/j.jmmm.2005.01.041>
- Han K-H, Bruno Frazier A (2004) Continuous magnetophoretic separation of blood cells in microdevice format. *J Appl Phys* 96(10):5797–5802. <http://aip.scitation.org/doi/10.1063/1.1803628>
- Han K, Frazier AB, Drive A (2005) A microfluidic system for continuous magnetophoretic separation of suspended cells using their native magnetic properties. *NSTI Nanotech* 1(Dmc):187–190

- Hoyos M et al (2000) Study of magnetic particles pulse-injected into an annular SPLITT-like channel inside a quadrupole magnetic field. *J Chromatogr A* 903(1–2):99–116. <http://linkinghub.elsevier.com/retrieve/pii/S0021967300008797>
- Inglis DW et al (2004) Continuous microfluidic immunomagnetic cell separation. *Appl Phys Lett* 85(21):5093–5095. <http://aip.scitation.org/doi/10.1063/1.1823015>
- Khashan SA et al (2017a) Microdevice for continuous flow magnetic separation for bioengineering applications. *J Micromech Microeng* 27(5):055016. <http://stacks.iop.org/0960-1317/27/i=5/a=055016?key=crossref.8df3a9a140b98851af479168478f8fb5>
- Khashan SA et al (2017b) Mixture model for biomagnetic separation in microfluidic systems. *J Magn Magn Mater* 442:118–127. <https://doi.org/10.1016/j.jmmm.2017.06.096>
- Khashan SA, Furlani EP (2012) Effects of particle–fluid coupling on particle transport and capture in a magnetophoretic microsystem. *Microfluid Nanofluidics* 12(1–4):565–580. <http://link.springer.com/10.1007/s10404-011-0898-y>
- Khashan SA, Furlani EP (2013) Coupled particle–fluid transport and magnetic separation in microfluidic systems with passive magnetic functionality. *J Phys D Appl Phys* 46(12):125002. <http://stacks.iop.org/0022-3727/46/i=12/a=125002?key=crossref.f265203de92addfb0f62dde8e86da09d>
- Khashan SA, Furlani EP (2014) Scalability analysis of magnetic bead separation in a microchannel with an array of soft magnetic elements in a uniform magnetic field. *Sep Purif Technol* 125:311–318. <http://link.springer.com/10.1007/s10404-011-0898-y>
- Khashan SA, Elnajjar E, Haik Y (2011) Numerical simulation of the continuous biomagnetic separation in a two-dimensional channel. *Int J Multiphase Flow* 37(8):947–955. <https://doi.org/10.1016/j.ijmultiphaseflow.2011.05.004>
- Khashan SA, Alazzam A, Furlani EP (2014) Computational analysis of enhanced magnetic bioseparation in microfluidic systems with flow-invasive magnetic elements. *Sci Rep* 4(1):5299. <http://www.nature.com/articles/srep05299>
- Khashan SA, Alazzam A, Furlani EP (2015) Computational analysis of enhanced magnetic bioseparation in microfluidic systems with flow-invasive magnetic elements. *Sci Rep* 4(1):5299. <http://www.ncbi.nlm.nih.gov/pubmed/24931437>
- Kim U, Soh HT (2009) Simultaneous sorting of multiple bacterial targets using integrated dielectrophoretic–magnetic activated cell sorter. *Lab Chip* 9(16):2313. <http://xlink.rsc.org/?DOI=b903950c>
- Kong TF et al (2011) An efficient microfluidic sorter implementation of double meandering microstriplines for magnetic particles switching. *Microfluid Nanofluidics* 10(5):1069–1078. <http://hdl.handle.net/10220/7731>
- Lou X et al (2009) Micromagnetic selection of aptamers in microfluidic channels. *Proc Natl Acad Sci* 106(9):2989–2994. <https://doi.org/10.1073/pnas.0813135106>
- McCloskey KE et al (2003) Magnetophoretic cell sorting is a function of antibody binding capacity. *Biotechnol Progress* 19(3):899–907. <http://doi.wiley.com/10.1021/bp020285e>
- McCloskey KE, Chalmers JJ, Zborowski M (2003) Magnetic cell separation: characterization of magnetophoretic mobility. *Anal Chem* 75(24):6868–6874. <http://www.ncbi.nlm.nih.gov/pubmed/14670047>
- Pamme N, Manz A (2004) On-chip free-flow magnetophoresis: continuous flow separation of magnetic particles and agglomerates. *Anal Chem* 76(24):7250–7256. <http://pubs.acs.org/doi/abs/10.1021/ac049183o>
- Ramadan Q, Poenar DP, Yu C (2009) Customized trapping of magnetic particles. *Microfluid Nanofluidics* 6(1):53–62. <http://link.springer.com/10.1007/s10404-008-0296-2>
- Vojtišek M et al (2012) Microfluidic devices in superconducting magnets: on-chip free-flow diamagnetophoresis of polymer particles and bubbles. *Microfluid Nanofluidics* 13(4):625–635. <http://link.springer.com/10.1007/s10404-012-0979-6>
- Ying TY, Yiacoumi S, Tsouris C (2000) High-gradient magnetically seeded filtration. *Chem Eng Sci* 55(6):1101–1113
- Zhang J et al (2014) Particle inertial focusing and its mechanism in a serpentine microchannel. *Microfluid Nanofluidics* 17(2):305–316. Available at: <http://link.springer.com/10.1007/s10404-013-1306-6>
- Zhang J et al (2016) A novel viscoelastic-based ferrofluid for continuous sheathless microfluidic separation of nonmagnetic microparticles. *Lab Chip* 16:3947–3956. <https://doi.org/10.1039/C6LC01007E>

Publisher's Note Springer Nature remains neutral with regard to jurisdictional claims in published maps and institutional affiliations.